POLITECNICO DI TORINO
Repository ISTITUZIONALE

Chaos and multi-layer attractors in asymmetric neural networks coupled with discrete fractional memristor

Availability:
This version is available at: 11583/2982623 since: 2023-09-30T09:33:43Z

Terms of use:

(Article begins on next page)

15 May 2024

Chaos and firing patterns in a discrete fractional Hopfield neural network model

Shaobo He · D. Vignesh · Lamberto Rondoni · Santo Banerjee

Abstract This article explores the importance of neuronal firing patterns in transmitting information within the human brain. These patterns are unique to each group of neurons and play a crucial role in understanding their diverse behavior. The article introduces various activation functions for neurons and develops a 4D discrete fractional-order Hopfield neural network model to showcase the complex dynamics involved. Additionally, the neurons exhibit non-linear behavior in their self synaptic weight functions due to external stimuli. The article examines the dynamics of the network with and without external stimulus, presenting bifurcation diagrams that illustrate the transition between chaotic and stable states. The research also investigates the region of chaos in relation to the fractional order and the non-linear synaptic function. The largest Lyapunov exponents are used to illustrate this chaotic region. It also demonstrates the network's sensitivity to even the smallest changes in parameter values, visualizing different firing patterns. This research emphasizes how the choice of activation functions, fractional order, and external input greatly influence the equilibrium and behavior of the network's state variables. By analyzing the system's dynamics and changes in equilibrium states over time, the study sheds light on the diverse dynamical characteristics exhibited by the system.

Shaobo He
School of Automation and Electronic Information, Xiangtan University, Xiangtan 411105, China
E-mail: heshaobo_123@163.com

D. Vignesh (Corresponding author)
Cyber Security and Digital Industrial Revolution Centre, Universiti Pertahanan Nasional Malaysia, Kem, Sungai Besi, 57000 Kuala Lumpur, Malaysia
E-mail: dvignesh260@gmail.com

Lamberto Rondoni, Santo Banerjee
Department of Mathematical Sciences, Giuseppe Luigi Lagrange, Politecnico di Torino, Corso Duca degli Abruzzi 24, Torino, Italy.
E-mail: lamberto.rondoni@polito.it, santoban@gmail.com

1 Introduction

The human brain, as the core of the nervous system, is responsible for controlling various bodily activities by processing sensory information. To understand the intricate information processing in the brain, researchers have developed artificial neural network models that mimic the behavior of neurons, which are the fundamental units of these models. These neural network models have found significant applications in diverse fields such as image and speech recognition, machine learning, medical diagnosis, stock market prediction, air patrols, drone control, weather forecasting, and more [10], [4], [23]. One of the key advantages of these models is their ability to learn from data samples to produce output, making them cost-effective alternatives to working with complete datasets. To comprehend the dynamics of the brain through these models, several scientific contributions have focused on analyzing the nonlinear characteristics and chaotic responses of these neural network models. These models, built on the foundation of neurons as the core computing units, employ activation functions that determine whether a neuron should fire and transmit signals to subsequent layers. These architectures have been extensively utilized in neural network designs featuring multiple hidden layers, with each layer possessing its specific activation function. Readers interested in stability and Hopf bifurcation in delay network models can refer to [38], [9], [14]. Li et al. [19] investigated a complex-valued model for neural networks and its dynamics with delay, while Cheng et al. [13] discussed stability and bifurcation in three-triangle network models. Those seeking an understanding of the chaotic behavior of neural networks can refer to [6], [40]. However, classical calculus-based models have certain limitations, such as the local nature of derivatives and the failure to consider past events, which can impact the accuracy and realization of these models.

Fractional calculus has emerged as a powerful tool in the twentieth century for accurately describing real-life processes compared to traditional derivative techniques. It involves generalizing the concept of derivative order to real or complex numbers. While the interpretation of these mathematical concepts was initially unclear, advancements in computing technology and theoretical knowledge have led to an increasing number of applications for fractional derivatives. Fractional derivatives have found applications in various fields such as physical and chemical engineering, ecology, medical research, security and communication networks, and electrical engineering. For instance, Shida et al. [28] applied fractional derivatives for climate prediction, Yang et al. [39] used them in image processing, and Magin [22] explored their utility in bioengineering. These applications demonstrate the capacity of fractional derivatives to incorporate memory factors into real-life models, making them particularly relevant for neural networks due to their association with memory. Researchers

have actively investigated the use of fractional derivatives in neural network models. Noteworthy contributions in this area include Xu et al. [37], who compared classical and fractional derivatives in neural networks, and studies analyzing the dynamical behavior of neural networks modeled with fractional derivatives [26], [31], [18], [17], [20]. Fractional differential neural networks have been particularly significant in system identification [5], [32], [21], while Zhang et al. [41] explored stability analysis in delay models, and Chen et al. [12] investigated global stability in terms of Mittag-Leffler stability. Overall, the integration of fractional derivatives into neural network models has garnered significant attention due to their ability to capture memory effects, leading to improved modeling and analysis capabilities in various domains.

Over the past two decades, discrete-time fractional calculus has experienced significant development and has become a focus of scientific interest for creating new models. The theory of discrete calculus has been supported by the works of Atici and Eloe [8], Goodrich [15], and Ostalczyk [24]. Furthermore, the discussion on tempered discrete fractional operators by Abdeljawad [3] and their applications in physical, biological, and chemical systems [27], [33], [34] have contributed to advancing the field. Regarding the application of discrete fractional operators in the modeling of neural network models, relevant literature includes [30], [7], where authors discuss and explore the dynamics of neural networks with discrete fractional operators. The work of [16] introduces variable-order discrete fractional operators and investigates their impact on network dynamics. Abbes et al. [1] analyze chaos in neural networks with incommensurate order operators, while Wu et al. [35] examine stability with respect to Mittag-Leffler functions. Additionally, the application of discrete fractional neural networks in heat transfer modeling is explored [29]. Most of the neural network models in literature are constructed with identical activation function to the network. Activation function introduces non-linearity to the neuron's output, allowing the network to learn and model complex relationships in the data. Considering two different activation functions in a neural network can offer several benefits. Some of the advantages are

1. Different activation functions possess distinct non-linear properties, and incorporating a variety of them enables the network to capture a broader range of non-linear patterns present in the data.
2. Various activation functions exhibit different characteristics and behaviors. Utilizing multiple activation functions allows the network to adapt and respond differently to different types of inputs, enhancing its capability to model diverse features and relationships within the data.
3. The choice of suitable activation functions can significantly impact the overall performance of the network. Certain activation functions may excel in specific scenarios or aid the network in overcoming particular challenges. By combining different activation functions, the network has the potential to achieve enhanced performance and accuracy.
4. The selection and arrangement of activation functions depend on the problem, network architecture, and data characteristics. Integrating different

activation functions in various ways enables customization to suit the specific requirements of the given task.

With a growing interest in the application of non-integer order operators in discrete time for network modeling, this article seeks to contribute to the existing literature by constructing a neural network model with discrete fractional operator. The primary goal is to explore the dynamical nature of network systems by incorporating different activation functions and nonlinear weight functions. The specific contributions of this article are as follows:

– The construction of a 4D neural network model that incorporates nonlinear self-synaptic weight functions and employs heterogeneous activation functions for the neurons.
– Consideration of both periodic (sine) and non-periodic (tanh) functions as activation functions for the neurons within the network.
– Analysis of stability and bifurcation phenomena to investigate the complex dynamical behavior of the system, supported by numerical simulations.
– Exploration of various firing patterns exhibited by the neural network model, including periodic and chaotic patterns. Additionally, investigation of the equilibrium shifting behavior of the network models.

The remaining sections of the article are organized as follows: Section 2 provides the necessary mathematical prerequisites for the study, establishing the foundational concepts required to understand the subsequent analysis. In Section 3, the mathematical formulation of the neural network model is presented, including its model structure represented in the form of a topological diagram. The qualitative nature of the proposed 4D model is analyzed using numerical simulations in Section 4 and Section 5. These sections examine the behavior and characteristics of the model, shedding light on its dynamics and properties. Section 6 focuses on the sensitivity behavior of the model, examining how small changes in parameter values impact its performance and behavior. Section 7 presents the investigation of various patterns exhibited by the model, specifically exploring bursting neurons and the switching of equilibrium states.

2 Prerequisites

In this section, we provide the essential mathematical definitions and theorems that are required for the analytical analysis in the article. Let $\mathbb{N}_\alpha = \{\alpha, \alpha + 1, \alpha + 2, \cdots\}$ such that $\alpha \in \mathbb{R}$.

Definition 1 [2] Consider a function $\phi : \mathbb{N}_\alpha \to \mathbb{R}$. $\upsilon-$ th order fractional sum is

$$\Delta_\alpha^{-\upsilon}\phi(\omega) = \frac{1}{\Gamma(\upsilon)} \sum_{r=\alpha}^{\omega-\upsilon} (\omega - r - 1)^{(\upsilon-1)} \phi(r), \tag{1}$$

where $\omega \in \mathbb{N}_{\alpha+\upsilon}, \upsilon > 0$.

Definition 2 [2]For $\phi : \mathbb{N}_\alpha \to \mathbb{R}$, the Caputo difference of arbitrary order υ is

$$
\begin{aligned}
{}^C\Delta_\alpha^\upsilon \phi(\omega) &= \Delta_\alpha^{-(\eta-\upsilon)} \Delta^\eta \phi(\omega) \\
&= \frac{1}{\Gamma(\eta-\gamma)} \sum_{r=\alpha}^{\omega-(\eta-\upsilon)} (\omega - r - 1)^{(\eta-\upsilon-1)} \Delta^\eta \phi(r),
\end{aligned}
\tag{2}
$$

where $\eta = [\upsilon] + 1$, $\upsilon > 0$, $\omega \in \mathbb{N}_{\alpha+\eta-\upsilon}$.

Theorem 1 *[25] Consider a fractional discrete time system of order υ*

$$
\begin{aligned}
{}^C\Delta_\alpha^\upsilon \phi(\omega) &= \mathcal{G}(\omega + \upsilon - 1, \phi(\omega + \upsilon - 1)), \\
\Delta^\eta \phi(\alpha) &= \phi_\eta, \delta = \lceil \upsilon \rceil + 1, \eta = 0, 1, 2, \ldots, \delta - 1,
\end{aligned}
\tag{3}
$$

then corresponding numerical form is

$$
\begin{aligned}
\phi(\omega) = \phi_0(\omega) + \frac{1}{\Gamma(\upsilon)} \sum_{r=\alpha+\delta-\upsilon}^{\omega-\upsilon} (\omega - r + 1)^{(\upsilon-1)} \\
\mathcal{G}(r + \upsilon - 1, \phi(r + \upsilon - 1)), \ \omega \in \mathbb{N}_{\upsilon+\delta},
\end{aligned}
\tag{4}
$$

with

$$
\phi_0(\omega) = \sum_{\eta=0}^{\delta-1} \frac{(\omega - \alpha)^{(\eta)}}{\Gamma(\eta+1)} \Delta^\eta \phi(\alpha).
\tag{5}
$$

Remark 1 Choosing the discrete kernel function $\sum\limits_{r=\alpha+\delta-\upsilon}^{\omega-\upsilon} (\omega - r + 1)^{(\upsilon-1)}$ as

$\dfrac{\Gamma(\omega - r)}{\Gamma(\upsilon)\Gamma(\omega - r - \upsilon + 1)}$ with assumption $\alpha = 0$ and $r + \upsilon = \alpha$, the numerical formula when $\upsilon \in (0, 1)$ is obtained as

$$
\phi(\omega) = \phi(0) + \frac{1}{\Gamma(\upsilon)} \sum_{\alpha=1}^{\omega} \frac{\Gamma(\omega - \alpha + \upsilon)}{\Gamma(\omega - \alpha + 1)} \mathcal{G}(\alpha - 1, \phi(\alpha - 1)).
\tag{6}
$$

Theorem 2 *[11] Let $\upsilon \in (0, 1)$ and the fractional difference system be given by*

$$
\Delta^\upsilon \Theta(\omega + 1 - \upsilon) = \Lambda \Theta(\omega), n = 0, 1, 2, \cdots,
\tag{7}
$$

where $\Lambda \in \mathbb{R}^{k \times k}$. Let

$$
U^\upsilon = \Big\{ \beta \in \mathbb{C} : |\beta| < \Big(2 \cos \Big(\frac{|arg\beta| - \pi}{2 - \upsilon} \Big) \Big)^\upsilon \ and \ |arg\beta| > \frac{\upsilon\pi}{2} \Big\}.
\tag{8}
$$

If all $\beta \in U^\upsilon$, then the system (7) is asymptotically stable and if $\beta \in \mathbb{C} \backslash cl(U^\upsilon)$ for any β then the system (7) is unstable.
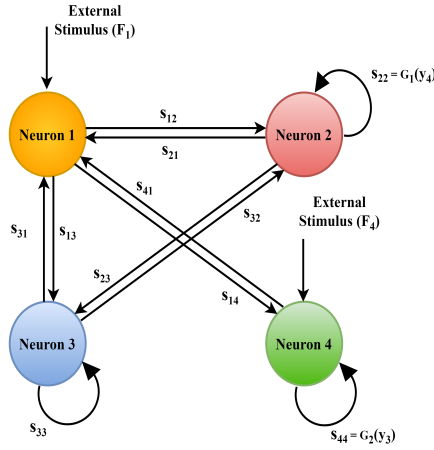
Fig. 1: Topological structure of 4D Hopfield Neural Networks with external stimuli

3 Discrete fractional Hopfield neural networks (HNN) model

Hopfield neural networks(HNNs) are most commonly employed for discussion on dynamics of brain.

General mathematical representation of the fractional order HNNs model [18] is given by

$$D^v y_i(\omega) = -d_i y_i(\omega) + \sum_{j=1}^{n} s_{ij} h_j(y_j(\omega)) + F_i, \qquad (9)$$

where D^v denotes the fractional operator, self regulatory factors of each neuron is denoted by d_i, connection strength between the ith and j^{th} neuron are represented by s_{ij} and the activation of neurons are represented by $h_j : \mathbb{R} \to \mathbb{R}$.

We now proceed with constructing a 4-D neural network model, as depicted in Figure 1, incorporating nonlinear synaptic weights. Synaptic weights in neural networks represent the strength of the connections between two neurons, and in a biological context, they play a crucial role in illustrating the influence of one neuron on another. To investigate the nonlinear dynamical characteristics of neuron behavior within the network, we will introduce non-linear activation functions to neuron 2 and neuron 4. These activation functions will demonstrate the input voltage levels in the neurons. In contemporary neural networks, popular activation functions include tanh, sigmoid, and ReLU, among others. However, for this study, we will introduce two different activation functions: tanh, a non-periodic function, and sine, a periodic function. The sine activation function holds significance as it introduces non-linearity when employed in a neural network, enabling the model to learn intricate patterns and relationships within the data. It proves advantageous in scenarios

where the data exhibits periodic or oscillatory patterns. The sine activation function excels in capturing periodic behavior, making it well-suited for tasks such as time series analysis or signal processing. Its ability to capture periodicity makes it a valuable tool in modeling and understanding cyclic phenomena within the data. The activation functions are given by $h_1(z) = h_3(z) = \sin z$ and $h_2(z) = h_4(z) = \tanh(z)$. Implementing the above consideration to the model (9) for four neurons, we get

$$
\begin{aligned}
D^v y_1(\omega) &= - y_1 + s_{12} \tanh(y_2) + s_{13} \sin(y_3) + s_{14} \tanh(y_4) + F_1, \\
D^v y_2(\omega) &= - y_2 + s_{21} \sin(y_1) + G_1(y_4) \tanh(y_2) + s_{23} \sin(y_3) + F_2, \\
D^v y_3(\omega) &= - y_3 + s_{31} \sin(y_1) + s_{32} \tanh(y_2) + s_{33} \sin(y_3) + F_3, \\
D^v y_4(\omega) &= - y_4 + s_{41} \sin(y_1) + G_2(y_3) \tanh(y_4) + F_4,
\end{aligned}
\tag{10}
$$

where nonlinear weight functions are $G_1(y_4) = (1 - \alpha_1 \tanh(y_4))$ and $G_2(y_3) = (\alpha_2 - \alpha_3 \sin(y_3))$, where $\alpha_1, \alpha_2, \alpha_3$ are real numbers and external stimuli $F_2 = 0$, $F_3 = 0$ with F_1, F_4 are positive real numbers. Article focuses on discussing the characteristics of the model with discrete fractional operator and discretizing (10) with Caputo fractional difference operator yields the model as follows.

$$
\begin{aligned}
\Delta_\kappa^v y_1(\omega) = &- y_1(\omega + v - 1) + s_{12} \tanh(y_2(\omega + v - 1)) \\
&+ s_{13} \sin(y_3(\omega + v - 1)) + s_{14} \tanh(y_4(\omega + v - 1)) + F_1, \\
\Delta_\kappa^v y_2(\omega) = &- y_2(\omega + v - 1) + s_{21} \sin(y_1(\omega + v - 1)) \\
&+ G_1(y_4(\omega + v - 1)) \tanh(y_2(\omega + v - 1)) + s_{23} \sin(y_3(\omega + v - 1)), \\
\Delta_\kappa^v y_3(\omega) = &- y_3(\omega + v - 1) + s_{31} \sin(y_1(\omega + v - 1)) \\
&+ s_{32} \tanh(y_2(\omega + v - 1)) + s_{33} \sin(y_3(\omega + v - 1)), \\
\Delta_\kappa^v y_4(\omega) = &- y_4(\omega + v - 1) + s_{41} \sin(y_1(\omega + v - 1)) \\
&+ G_2(y_3(\omega + v - 1)) \tanh(y_4(\omega + v - 1)) + F_4,
\end{aligned}
\tag{11}
$$

where Δ_κ^v represents the Caputo difference operator of order $0 < v \leq 1$, $y_1, y_2, y_3, y_4 \in \mathbb{R}^4$, $\omega \in \mathbb{N}_{\kappa+1-v}$. The main advantage of choosing the Caputo fractional difference operator over the Riemann-Liouville operator is that models constructed with the Caputo operator utilize integer order initial states, whereas the Riemann-Liouville operator requires fractional order initial states. We now employ fractional sum equations [25] with $\kappa = 0$ to obtain the numer-

ical form as

$$
\begin{aligned}
y_1(\omega) =& y_1(0) + \frac{1}{\Gamma(\upsilon)} \sum_{r=1}^{\omega} \frac{\Gamma(\omega - r + \upsilon)}{\Gamma(\omega - r + 1)} \bigg(-y_1(r-1) + s_{12}\tanh(y_2(r-1)) \\
& + s_{13}\sin(y_3(r-1)) + s_{14}\tanh(y_4(r-1)) + F_1 \bigg), \\
y_2(\omega) =& y_2(0) + \frac{1}{\Gamma(\upsilon)} \sum_{r=1}^{\omega} \frac{\Gamma(\omega - r + \upsilon)}{\Gamma(\omega - r + 1)} \bigg(-y_2(r-1) + s_{21}\sin(y_1(r-1)) \\
& + G_1(y_4(r-1))\tanh(y_2(r-1)) + s_{23}\sin(y_3(r-1)) \bigg), \\
y_3(\omega) =& y_3(0) + \frac{1}{\Gamma(\upsilon)} \sum_{r=1}^{\omega} \frac{\Gamma(\omega - r + \upsilon)}{\Gamma(\omega - r + 1)} \bigg(-y_3(r-1) + s_{31}\sin(y_1(r-1)) \\
& + s_{32}\tanh(y_2(r-1)) + s_{33}\sin(y_3(r-1)) \bigg), \\
y_4(\omega) =& y_4(0) + \frac{1}{\Gamma(\upsilon)} \sum_{r=1}^{\omega} \frac{\Gamma(\omega - r + \upsilon)}{\Gamma(\omega - r + 1)} \bigg(-y_4(r-1) + s_{41}\sin(y_1(r-1)) \\
& + G_2(y_3(r-1))\tanh(y_4(r-1)) + F_4 \bigg), \quad \omega = 1, 2, \cdots .
\end{aligned}
\tag{12}
$$

The actual performance and advantages of a 4-neuron model over a 3-neuron model would need to be evaluated empirically in the context of a particular problem. But some advantages of considering 4-neuron network model are presented as follows.

1. Enhanced Complexity: By including an extra neuron, the model becomes capable of representing more intricate patterns and processing data in a more sophisticated manner.
2. Improved Representation: Neural networks with a higher number of neurons have the potential to capture a broader range of input data, leading to a more comprehensive understanding of the information being processed.
3. Flexibility and Optimization: The inclusion of an additional neuron allows for greater flexibility in adjusting the model's architecture and optimizing its performance for specific tasks, enabling more effective fine-tuning.

4 Neural network model without external stimulus

This section depicts the results on qualitative behavior of the HNNs (11) without external stimulus, as in Figure 2, via stability conditions from eigenvalues at their equilibrium position, transition of states of the model with bifurcation diagrams for fractional order (υ) and α_2 together with largest Lyapunov exponents using Jacobian matrix method proposed in [36].
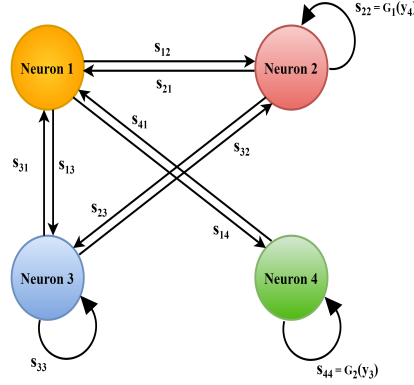
Fig. 2: Topological structure of 4D Hopfield Neural Networks with $F_1 = F_4 = 0$

4.1 Stability Analysis

Stability analysis of the neural network model presented in (**??**) without external inputs ($F_1 = F_4 = 0$) is performed by numerical evaluation of eigenvalues at their equilibrium states. Let the parameters take the values $\alpha_1 = -0.5$, $\alpha_2 = 1$, $\alpha_3 = 0.5$, $s_{12} = -0.4$, $s_{13} = 0.2$, $s_{14} = 3$, $s_{21} = -0.5$, $s_{23} = 1.3$, $s_{31} = 1$, $s_{32} = -0.8$, $s_{33} = 0.2$, $s_{41} = 1.4$ with initial state $(0.8, 0.3, 0.4, 0.6)$ and fractional order $\upsilon = 0.7$. The equilibrium states of the system for the assumed parameters value are

1. $P_0 = (0, 0, 0, 0)$,
2. $P_1 = (-2.71954, -0.26150, -0.25563, -1.61402)$,
3. $P_2 = (2.56077, 0.71928, 0.06940, 1.66706)$.

Jacobian matrix of the system (11) at P_2 is obtained as

$$H(P_2) = \begin{bmatrix} -1 & -0.24798 & 0.19951 & 0.39880 \\ 0.41800 & -0.09138 & 1.29686 & 0.04097 \\ -0.83601 & -0.49597 & -0.80048 & 0 \\ -1.17041 & 0 & -0.46446 & -0.87167 \end{bmatrix} \tag{13}$$

and the corresponding eigenvalues are $\beta_{1,2} = -0.9376828045 \pm i\, 1.023807399$, $\beta_{3,4} = -0.4440857426 \pm i\, 0.4519528532$. We have a pair of conjugate complex eigenvalues and following conditions from Theorem 2 has to be verified.

(E_1) $|\beta| < \left(2\cos\left(\frac{|arg\beta| - \pi}{2 - \upsilon}\right)\right)^{\upsilon}$,

(E_2) $|arg\beta| > \dfrac{\upsilon\pi}{2}$.

Absolute values of the eigenvalues are

$$\begin{aligned} |-0.9376828045 \pm i\, 1.023807399| &= 1.388319355, \\ |-0.4440857426 \pm i\, 0.4519528532| &= 0.6336193876. \end{aligned} \tag{14}$$

and

$$\left(2\cos\left(\frac{|arg\beta_{1,2}| - \pi}{1.3}\right)\right)^{0.7} = 1.392941487$$
$$\left(2\cos\left(\frac{|arg\beta_{3,4}| - \pi}{1.3}\right)\right)^{0.7} = 1.412082905 \tag{15}$$

Hence, from (14) and (15) condition E_1 is satisfied. For the case of E_2,

$$|argument(-0.9376828045 \pm i\ 1.023807399)| = 2.31231,$$
$$|argument(-0.4440857426 \pm i\ 0.4519528532)| = 2.34741. \tag{16}$$

and with $\upsilon = 0.7$, we have $\dfrac{0.7\pi}{2} = 1.1$. Therefore, it is evident that $|argument(\beta_{1,2,3,4})| < 1.1$ and condition E_2 is satisfied. Numerical evaluation supports the condition for stability proposed in Theorem 2 and system (11) is asymptotically stable at equilibrium state P_2 as visualized in Fig 3. The stability nature of the other two equilibrium states are presented in Table 1.
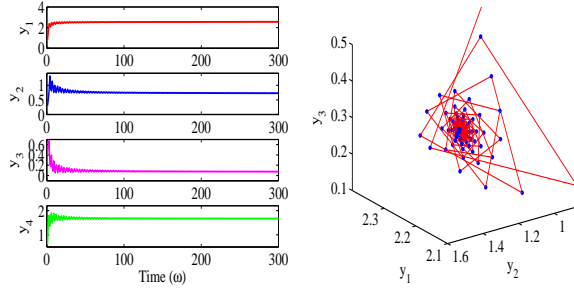
Fig. 3: Asymptotic stability at equilibrium state P_2.

4.2 Fractional order dependent Chaotic dynamics

In this section, we analyze the chaotic behavior of the network model (**??**) in the absence of external inputs. We interpret this behavior by studying bifurcation diagrams while varying the fractional order (υ). The parameter values remain fixed as discussed in section 4.1, and we explore fractional orders within the range $0 < \upsilon \leq 1$. By examining the bifurcation diagrams, we observe the dynamic changes in the qualitative characteristics of the system due to the influence of the fractional order. Figure 4 illustrates the bifurcation diagrams for each state variable, depicting the system's behavior as the fractional order varies. The chaotic zones are demonstrated with largest Lyapunov exponents

Table 1: Stability nature at equilibrium states

Fixed point	Eigenvalues	Nature of stability	
P_0	$\beta_1 = -2.745650252$ $\beta_2 = 1.63825$ $\beta_3 = -0.34630 + i\,0.92258$ $\beta_4 = -0.34630 - i\,0.92258$	Unstable	$arg(1.63825) = 0$ (E_2) fails
P_1	$\beta_1 = -0.83959 + i\,1.18960$ $\beta_2 = -0.83959 - i\,1.18960$ $\beta_3 = -0.72957 + i\,0.61182$ $\beta_4 = -0.72957 - i\,0.61182$	Unstable	$\left(2\cos\left(\frac{|arg\beta_{1,2}|-\pi}{1.3}\right)\right)^{0.7} = 1.31679$ $abs(\beta_{1,2}) = 1.45604$ (E_1) fails
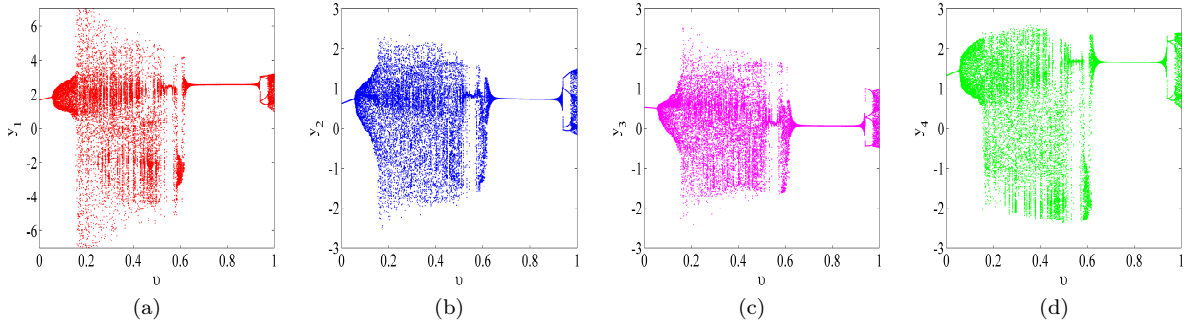
Fig. 4: Bifurcation diagrams with varying fractional order $0 < \upsilon \le 1$.
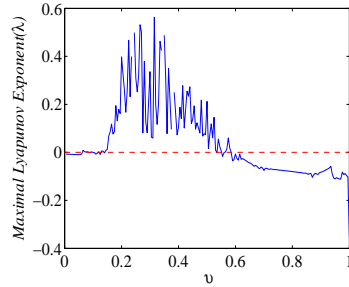
Fig. 5: Largest Lyapunov exponent corresponding to bifurcation diagrams in Fig 4.

in Fig 5. The neural network system with fractional order υ close to zero exhibits a stable behavior and switches to chaos for gradual increase of υ. In Figure 4, the chaotic region is depicted using scattered plots in the bifurcation diagram. Additionally, a phase space view is presented in Figure 6(b). When
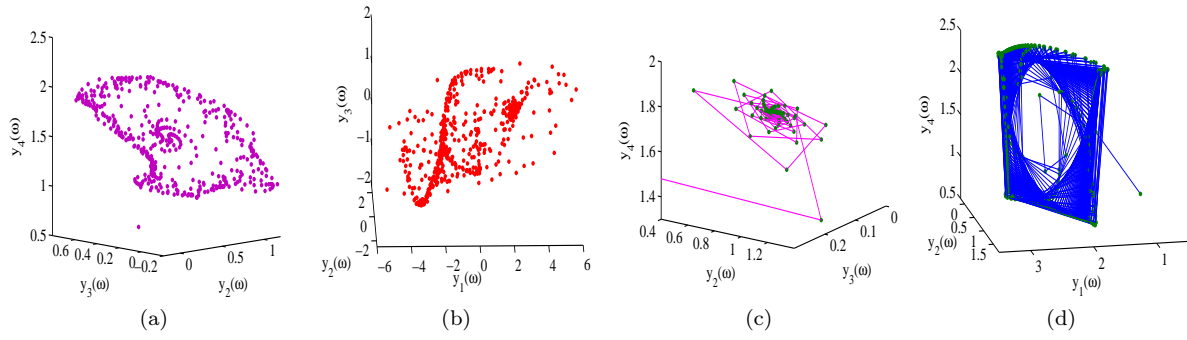
Fig. 6: Phase plane plots for bifurcation diagrams Fig 4.

the fractional order υ exceeds 0.5, the system undergoes a transformation into a stable region, as evidenced by the largest Lyapunov exponents shown in Figure 5. An interesting observation is that as the fractional order approaches 1, the system exhibits a shift in behavior from a stable spiral phase plane to the formation of closed orbits, as depicted in Figure 6(d).
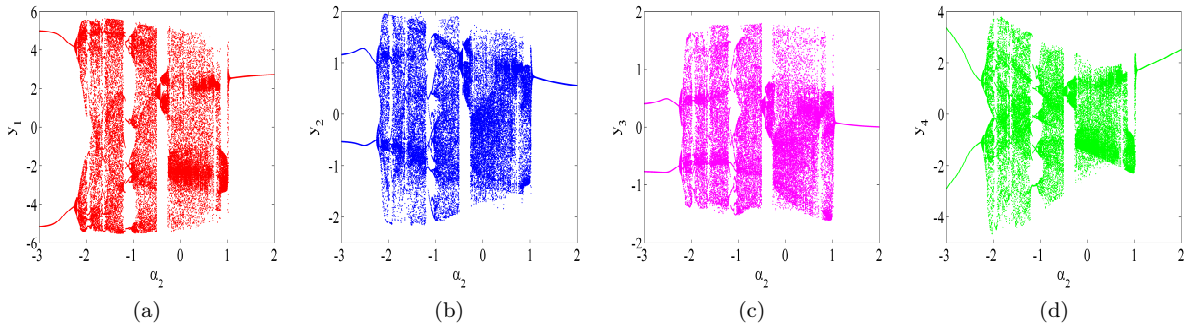
4.3 Dynamics based on parameter α_2

Fig. 7: Bifurcation diagrams with varying $-3 < \alpha_2 \leq 2$.

While examining the qualitative aspects of the system's behavior based on a common parameter for all state variables, it is important to note that it does not provide a complete narrative of the inter-relationships between the connected neurons. To gain a deeper understanding of these associations, we focus our discussion on the influence of the parameter α_2 within the nonlinear weight function of neuron y_4. In order to explore this topic, numerical simu-

lations are conducted using the same parameter values as in section 4.1, with $v = 0.6$ and α_2 varying within the range of $[-3, 2]$.
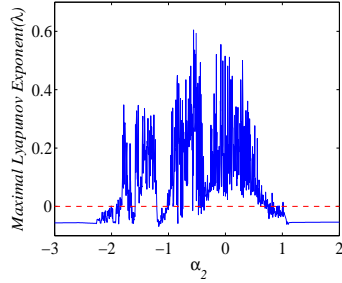

Fig. 8: Largest Lyapunov exponent corresponding to bifurcation diagrams in Fig 7.
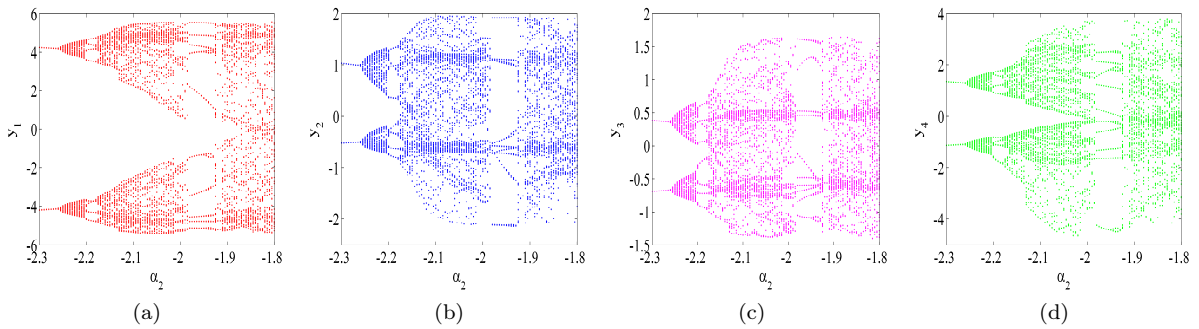

Fig. 9: Amplification of bifurcation diagrams with varying $-2.3 < \alpha_2 \leq -1.8$.

The parameter α_2, which defines the nonlinear synaptic weight of neuron y_4, introduces interesting qualitative changes to the system, as depicted in Figure 7. When α_2 lies within the range of $[-3, 0.4)$, the system exhibits symmetric bifurcation about the origin, merging together and displaying complex dynamics. For values of α_2 between $[-0.4, 2]$, the system's behavior is characterized by a single large region of bifurcation. The symmetric behavior observed in the bifurcation diagrams can be further observed in the phase plane plots shown in Figure 10. When examining the phase plane plot in Figure 11, the system follows an equilibrium position, indicating the uniform oscillatory nature of the neural network. These complex dynamics exhibited by the system are supported by the largest Lyapunov exponents shown in Figure 8. The
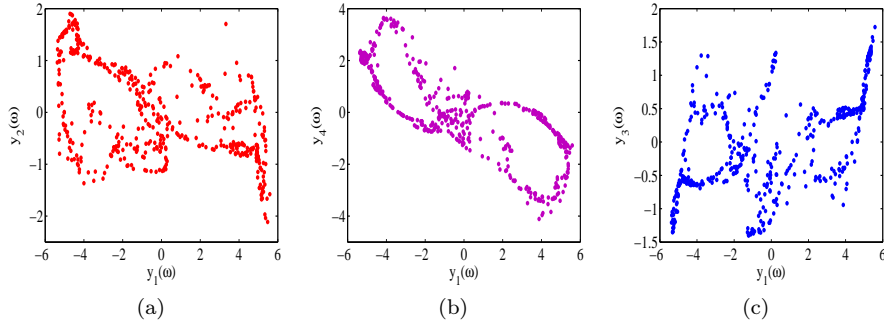
Fig. 10: Phase plane plots corresponding to bifurcation diagrams in Fig 7 for $\alpha_2 = -1.725$.
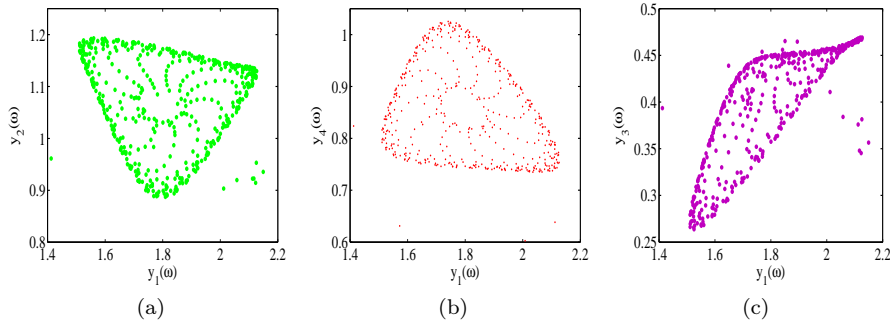

Fig. 11: Phase plane plots corresponding to bifurcation diagrams in Fig 7 for $\alpha_2 = -0.5$.

periodic doubling characteristics of the neural network system are explored through an amplified version of the bifurcations, as presented in Figure 9.

4.4 Coexisting bifurcation and attractors

Investigation of the coexistence behaviour of the attractors illustrates the dynamical evolution of the system with variation in parameters and initial states of the state variables of the dynamical system. Coexistence of the system states is investigated with fixed values of parameters as $\alpha_1 = 0.2$, $\alpha_2 = 0.4$, $\alpha_3 = 0.5$, $s_{12} = -0.4$, $s_{13} = 0.2$, $s_{14} = 1.72$, $s_{21} = -1$, $s_{23} = 1.3$, $s_{31} = 0.6$, $s_{32} = 0.8$, $s_{33} = 0.9$, $s_{41} = 1.4$ varying fractional order υ between 0 and 1. Bifurcations in Fig 12 are simulated for two initial states: $Y_0 = (1, 2, 0.8, 0.6)$ represented in red colour and $Y_1 = (0.8, 1.2, -1.4, 0.6)$ in blue colour. The following observations are made from the coexisting bifurcations:
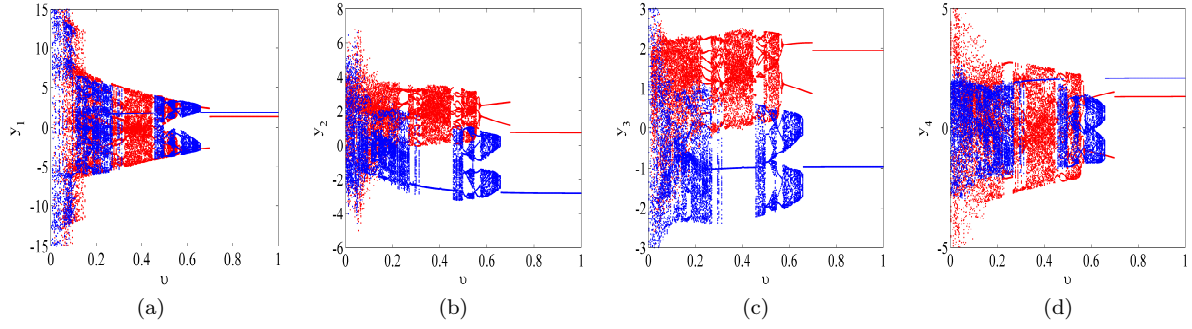
Fig. 12: Coexisting bifurcation diagrams with different initial conditions.

1. The proposed model, in the absence of external inputs or stimuli, exhibits high sensitivity to changes in initial conditions.
2. Under the initial state Y_0, the system gradually transitions from a chaotic state to stable behavior, forming periodic windows, as shown in Figure 12 (indicated in red).
3. When considering the system under the initial state Y_1 with the same set of parameters, a sudden switch from chaotic dynamics to stability can be observed for $\upsilon \in [0.2, 0.4]$. After achieving stability, the system experiences abrupt excitation leading to the formation of periodic windows and gradually returning to stability.
4. It is evident that the network model undergoes complex dynamical changes depending on its initial state.

To further expand our understanding of the coexisting behavior of the state variables, we investigate the changes that occur with varying system parameters. Using the same parameter set mentioned above, we study 3-dimensional phase plane plots for the initial states Y_0 and Y_1 while fixing $\upsilon = 0.2$. The plots are shown in Figure 13(a),(b) for $\alpha_2 = -1$ and in Figure 13(c),(d) for $\alpha_2 = -2$. Figure 13(c),(d) demonstrates the switching behavior between two equilibrium states, represented along the positive and negative axes, respectively. By increasing the fractional order to $\upsilon = 0.3, 0.4, 0.5$ and considering different pairs of α_2 values, coexisting attractors are presented in Figures 14, 15, 16 in the $y_1 - y_2 - y_3$ plane and the $y_2 - y_3 - y_4$ plane, respectively. The purpose of constructing various pairs of coexisting attractors is to investigate the dynamical changes of the neurons and their sensitivity to different initial states. The observation of coexisting attractors reveals that as the fractional order increases, the combined wings of the attractors split up, transitioning from $\upsilon = 0.3$ to separated attractors for $\upsilon = 0.5$. The study of coexisting attractors provides a better understanding of the system dynamics under different initial states.
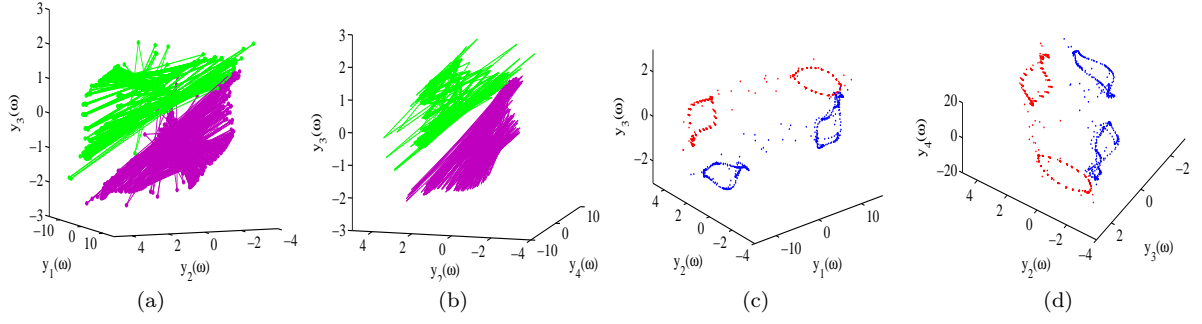
Fig. 13: Phase plane plots illustrating coexisting behavior (a),(b) $v = 0.2$, $\alpha_2 = -1$ along $y_1 - y_2 - y_3$ plane, (c),(d) $v = 0.2$, $\alpha_2 = -2$ along $y_2 - y_3 - y_4$ plane.
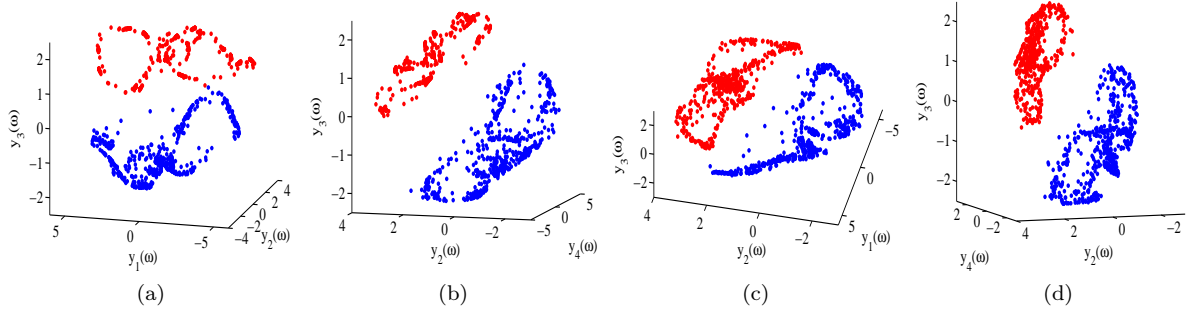

Fig. 14: Phase plane plots illustrating coexisting behavior (a),(b) $v = 0.3$, $\alpha_2 = 0.4$ along $y_1 - y_2 - y_3$ plane , (c),(d) $v = 0.3$, $\alpha_2 = 0.6$ along $y_2 - y_3 - y_4$ plane.

5 HNN model with identical external stimulus

5.1 Stability Analysis

Stability analysis of the neural network model presented in (11) with external inputs $(I_1 \neq 0, I_4 \neq 0)$ is performed by numerical evaluation of eigenvalues at their equilibrium states. Let the parameters take the values $\alpha_1 = -0.5$, $\alpha_2 = 1$, $\alpha_3 = 0.5$, $s_{12} = -0.4$, $s_{13} = 0.2$, $s_{14} = 3$, $s_{21} = -0.5$, $s_{23} = 1.3$, $s_{31} = 1$, $s_{32} = -0.8$, $s_{33} = 0.2$, $s_{41} = 1.4$ with initial state $(0.8, 0.3, 0.4, 0.6)$ and fractional order $v = 0.7$. The equilibrium states of the system for the assumed parameter values in three cases are as follows

Case - I $I_1 = I_4 = 0.01$.
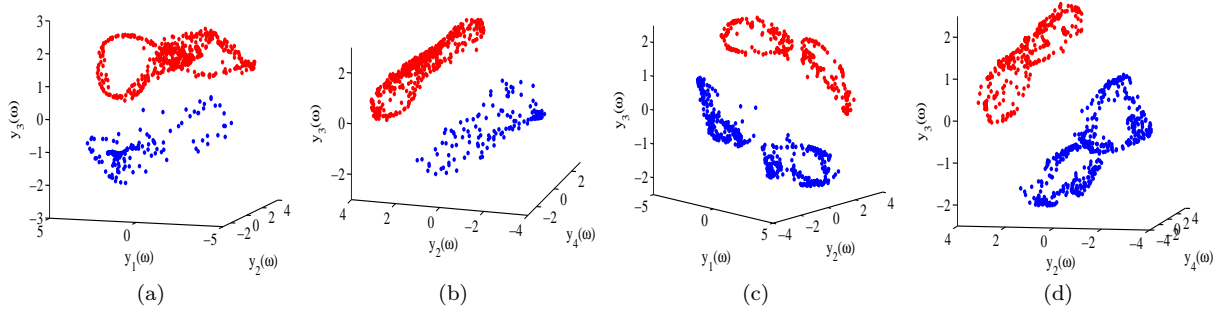   – $P_1' = (-0.00713, -0.00616, -0.00275, -0.00634)$,

Fig. 15: Phase plane plots illustrating coexisting behavior (a),(b) $v = 0.4$, $\alpha_2 = 0.4$ along $y_1 - y_2 - y_3$ plane, (c),(d) $v = 0.4$, $\alpha_2 = 0.65$ along $y_2 - y_3 - y_4$ plane.
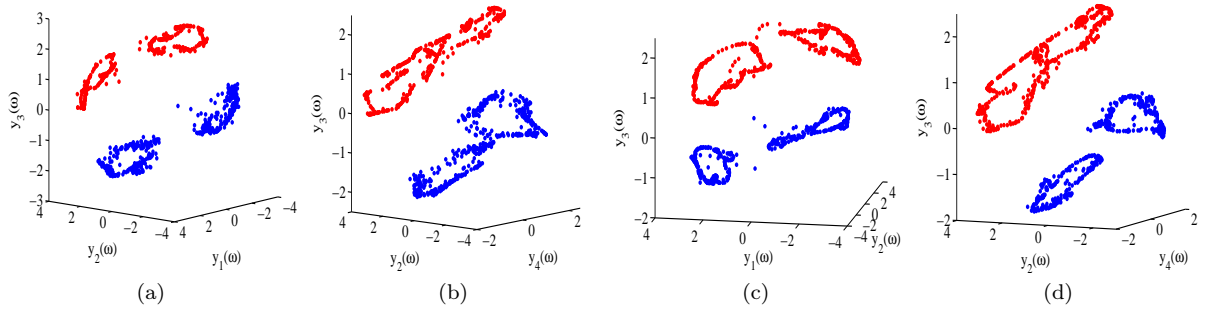

Fig. 16: Phase plane plots illustrating coexisting behavior (a),(b) $v = 0.5$, $\alpha_2 = 0.6$ along $y_1 - y_2 - y_3$ plane, (c),(d) $v = 0.5$, $\alpha_2 = 0.8$ along $y_2 - y_3 - y_4$ plane.

$$- \; P_2' = (-2.71062, -0.26662, -0.26096, -1.61850),$$
$$- \; P_3' = (2.57226, 0.70712, 0.06494, 1.66542).$$

Case - II $I_1 = 0.1 < I_4 = 0.4$.

$$- \; P_1'' = (-2.52665, -0.37038, -0.36479, -1.46704),$$
$$- \; P_2'' = (2.77715, 0.47939, -0.00022, 1.85093),$$
$$- \; P_3'' = (-0.28369, -0.22974, -0.12402, -0.15089).$$

Case - III $I_1 = 0.4 > I_4 = 0.1$.

$$- \; P_1''' = (-0.07073, -0.05757, -0.03083, -0.16397),$$
$$- \; P_2''' = (-2.41675, -0.41639, -0.43156, -1.99329),$$
$$- \; P_3''' = (2.87992, 0.33451, 0.00079, 1.33142).$$

The numerical result for the stability of the system (11) for Case-II ($I_4 > I_1$) is presented, and the rest of the cases will be tabulated. Jacobian matrix at P_{II2} is obtained as

$$H(P_2'') = \begin{bmatrix} -1 & -0.32051 & 0.19999 & 0.28203 \\ 0.46716 & 0.18265 & 1.29999 & 0.02095 \\ -0.93432 & -0.64103 & -0.80000 & 0 \\ -1.30805 & 0 & -0.47591 & -0.90597 \end{bmatrix} \quad (17)$$

Eigenvalues corresponding to matrix (17) are $\beta_{1,2} = -0.8566916615 \pm i\, 0.9960732964$ and $\beta_{3,4} = -0.4049718290 \pm i\, 0.4444650264$. Our aim is to verify the conditions (E_1) and (E_2) defined in Section 4.1.

The absolute values of the eigenvalues are

$$\begin{aligned} |-0.8566916615 \pm i\, 0.9960732964| &= 1.313804633, \\ |-0.4049718290 \pm i\, 0.4444650264| &= 0.6012913952. \end{aligned} \quad (18)$$

and

$$\begin{aligned} \left(2\cos\left(\frac{|arg\beta_{1,2}| - \pi}{1.3} \right) \right)^{0.7} &= 1.375226734 \\ \left(2\cos\left(\frac{|arg\beta_{3,4}| - \pi}{1.3} \right) \right)^{0.7} &= 1.391501628 \end{aligned} \quad (19)$$

Hence, from (18) and (19) condition E_1 is satisfied. For the case of E_2,

$$\begin{aligned} |argument(-0.8566916 \pm i\, 0.9960732)| &= 2.28110, \\ |argument(-0.4049718 \pm i\, 0.4444650)| &= 2.30973. \end{aligned} \quad (20)$$

and with $\upsilon = 0.7$, we have $\frac{0.7\pi}{2} = 1.1$. Therefore, it is evident that $|argument(\beta_{1,2,3,4})| < 1.1$ and condition E_2 is satisfied. Numerical evaluation supports the condition for stability proposed in Theorem 2 and system (11) is asymptotically stable at equilibrium state P_2 as visualized in Fig 17. The stability nature of the other two equilibrium states is presented in Table 2.
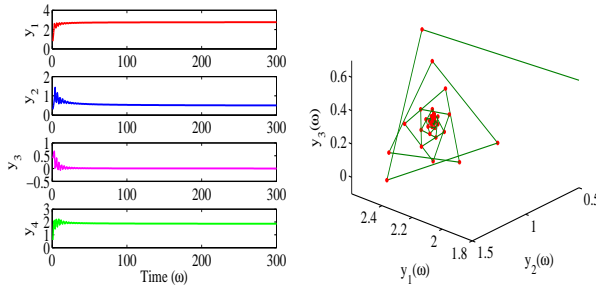

Fig. 17: Asymptotic stability at equilibrium state P_2.

Table 2: Stability nature at equilibrium states

Fixed point	Eigenvalues	Nature of stability	
Case - I ($I_1 = I_4 = 0.01$)			
P_1'	$\beta_1 = -2.74433$ $\beta_2 = 1.64017$ $\beta_3 = -0.34885 + i\ 0.92342$ $\beta_4 = -0.34885 - i\ 0.92342$	Unstable	$arg(1.64017) = 0$ (E_2) fails
P_2'	$\beta_1 = -0.83981 + i\ 1.18590$ $\beta_2 = -0.83981 - i\ 1.18590$ $\beta_3 = -0.73079 + i\ 0.60878$ $\beta_4 = -0.73079 - i\ 0.60878$	Unstable	$\left(2\cos\left(\frac{|arg\beta_{1,2}|-\pi}{1.3}\right)\right)^{0.7} = 1.31781$ $|\beta_{1,2}| = 1.45315$ (E_1) fails
P_3'	$\beta_1 = -0.93599 + i\ 1.02866$ $\beta_2 = -0.93599 - i\ 1.02866$ $\beta_3 = -0.43861 + i\ 0.45444$ $\beta_4 = -0.43861 - i\ 0.45444$	Stable	E_1 and E_2 are satisfied
Case - II ($I_1 = 0.1 < I_4 = 0.4$)			
P_1''	$\beta_1 = -0.82631 + i\ 1.14498$ $\beta_2 = -0.82631 - i\ 1.14498$ $\beta_3 = -0.72658 + i\ 0.66185$ $\beta_4 = -0.72658 - i\ 0.66185$	Unstable	$\left(2\cos\left(\frac{|arg\beta_{1,2}|-\pi}{1.3}\right)\right)^{0.7} = 1.32353$ $|\beta_{1,2}| = 1.41201$ (E_1) fails
P_3''	$\beta_1 = -2.64761$ $\beta_2 = 1.62741$ $\beta_3 = -0.43266 + i\ 0.92300$ $\beta_4 = -0.43266 - i\ 0.92300$	Unstable	$arg(1.62741) = 0$ E_2 fails
Case - III ($I_1 = 0.4 > I_4 = 0.1$)			
P_1'''	$\beta_1 = -2.70339$ $\beta_2 = 1.62761$ $\beta_3 = -0.41001 + i\ 0.92922$ $\beta_4 = -0.41001 - i\ 0.92922$	Unstable	$arg(1.62761) = 0$ (E_2) fails
P_2'''	$\beta_1 = -0.84845 + i\ 1.03475$ $\beta_2 = -0.84845 - i\ 1.03475$ $\beta_3 = -0.79853 + i\ 0.40292$ $\beta_4 = -0.79853 - i\ 0.40292$	Stable	E_1 and E_2 are satisfied
P_3'''	$\beta_1 = -0.92286 + i\ 1.30818$ $\beta_2 = -0.92286 - i\ 1.30818$ $\beta_3 = -0.21253 + i\ 0.57089$ $\beta_4 = -0.21253 - i\ 0.57089$	Stable	$\left(2\cos\left(\frac{|arg\beta_{1,2}|-\pi}{1.3}\right)\right)^{0.7} = 1.31665$ $|\beta_{1,2}| = 1.60094$ (E_1) fails

5.2 Dynamics based on parameter α_2

This section focuses on the results of the model with varying external inputs, specifically α_2, in relation to the complex dynamics discussed in Section 4.3. Bifurcation diagrams, depicted in Figure 18, are constructed using the same parameter values as in Section 4.1, where the external inputs F_1 and F_4 are set to 0.2. To provide a more detailed analysis, the amplification of different bifurcation regions is presented in Figures 20 and 21. Examining Figure 20,
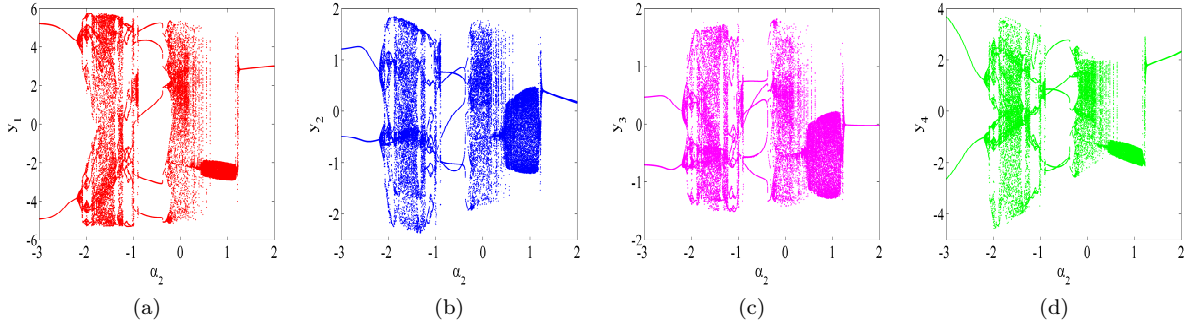
Fig. 18: Bifurcation diagrams with varying $-3 < \alpha_2 \leq 2$ and $F_1 = F_4$.

which covers the range of α in [-2.3,1.8], it can be observed that the bifurcations exhibit symmetry around 0. A complete cycle of system transitions, starting from a stable state and progressing to chaos through periodic oscillations, and vice versa, can be observed for values of α_2 ranging from [-2.08,-1.9]. Following this complete transformation, five bifurcations occur for α_2 within the range of [-1.4,-1.37].
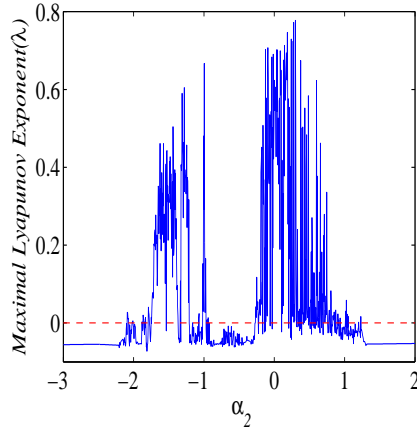

Fig. 19: Largest Lyapunov exponent corresponding to bifurcation diagrams in Fig 18.

The presence of chaotic regions in the system is accompanied by the emergence of periodic windows, leading to a systematic shift in the behavior of the system. This regular shift can be observed by examining the largest Lyapunov exponents shown in Figure 19. In Figure 22, the chaotic response at $\alpha_2 = -1.7$ and the uniform oscillatory response at $\alpha_2 = 1$ are presented. These figures
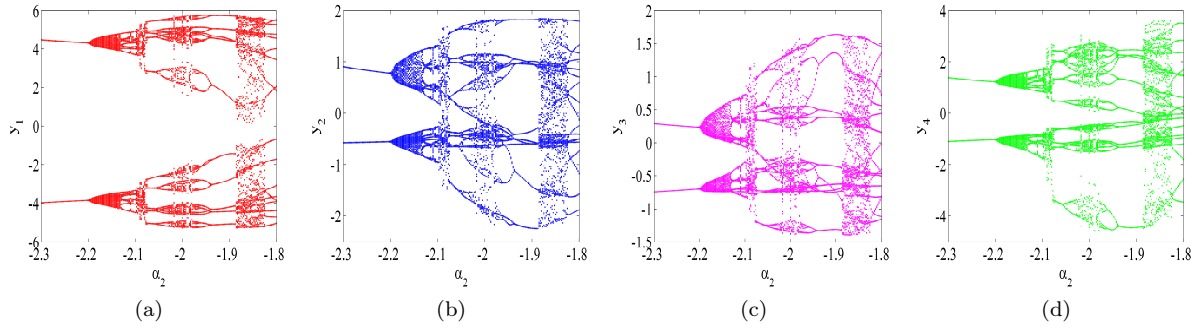
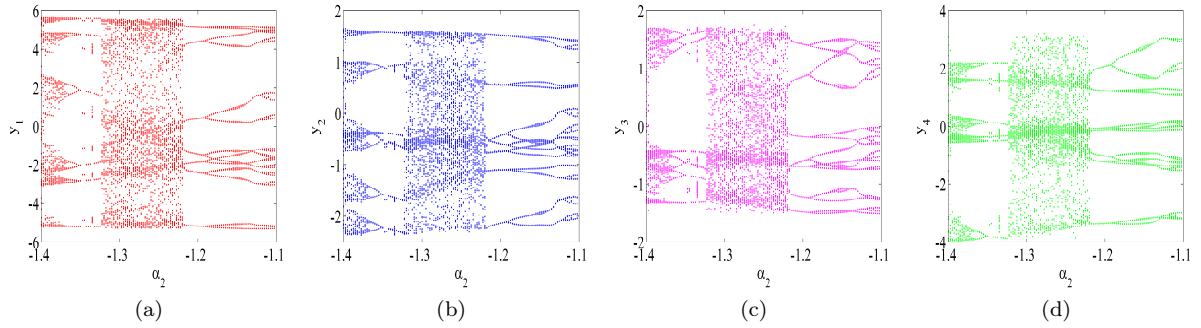Fig. 20: Amplification of bifurcation diagrams with varying $-2.3 < \alpha_2 \le -1.8$ and $F_1 = F_4$

Fig. 21: Amplification of bifurcation diagrams with varying $-1.4 < \alpha_2 \le -1.1$ and $F_1 = F_4$

provide visual representations of the dynamics observed in the system, high-lighting the coexistence of chaotic and oscillatory behaviors for different values of α_2.

The results comparing the complex dynamics of neural networks with distinct external stimuli are illustrated as follows:

1. In Section 5.2, the bifurcations are explored for the case of equal stimuli, where $F_1 = F_4 = 0.2$. However, a question arises regarding the impact of distinct stimulus values. To address this question, a series of bifurcation diagrams for each state variable is presented in Figure 23. The external stimuli F_1 is varied in the range of $[0, 1]$, while F_4 is fixed at values of 0.05, 0.2, and 0.5. The remaining parameters are held constant: $\alpha_1 = 0.2$, $\alpha_2 = 0.5$, $\alpha_3 = 0.5$, $s_{12} = -0.4$, $s_{13} = 0.2$, $s_{14} = 1.72$, $s_{21} = -1$, $s_{23} = 1.3$, $s_{31} = 0.6$, $s_{32} = 0.8$, $s_{33} = 0.9$, $s_{41} = 1.4$. The system's initial state is set to $(0.8, 1.2, 0.4, 0.6)$, and the fractional order is $\upsilon = 0.3$.
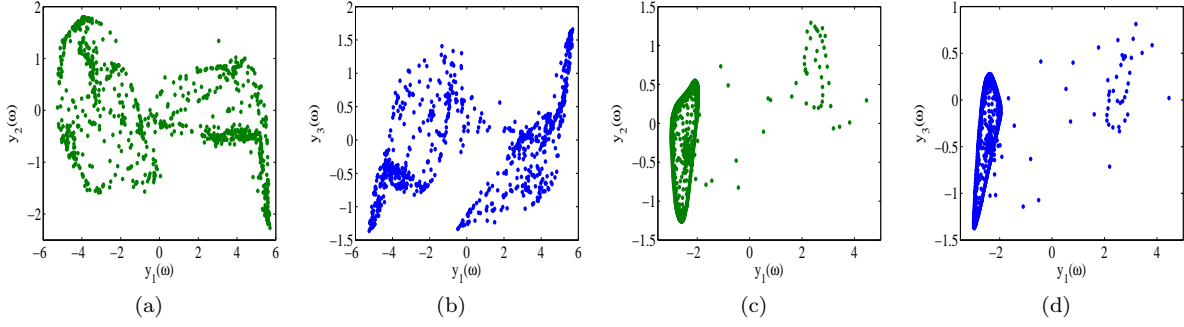
Fig. 22: Phase plane plots corresponding to bifurcation diagrams in Fig 18 – (a),(b) for $\alpha_2 = -1.7$ (c), (d) for $\alpha_2 = 1$.

2. A detailed analysis of the multiple 2D bifurcations presented in Figure 23 emphasizes the significance of external stimuli in controlling chaos. It is observed that smaller values of the stimulus lead to more chaotic behavior in the system, while higher stimulus values result in stabilization of the network model for the given parameter values. This interpretation provides a broader understanding of the impact of the parameters. Further analysis will be conducted under different scenarios to gain more insights.
3. The interpretations based on the external inputs for the given parameter values are as follows:
   – Scenario I: Assuming identical inputs for neurons 2 and 4, the system exhibits chaotic responses when $F_1 = F_4 < 0.35$, while stability behavior is observed when $F_1 = F_4 > 0.35$.
   – Scenario II: Allowing for non-identical inputs, contrasting values of inputs are required to exhibit chaotic or stable behavior. For the system to be chaotic, an increase in F_1 within the range of $(0, 0.5]$ should be accompanied by smaller values of F_4. For example, if $F_1 = 0.5$, the system is chaotic for $F_4 \in (0, 0.15)$. Similarly, for $F_4 = 0.05$, the system exhibits chaos for any choice of $F_1 \in (0, 0.5]$. The system remains stable for other combinations of input values.

6 Sensitivity behavior of the neural network model

The results obtained on the sensitivity of the proposed model align with the focus of this section of the article. In Section 4.3, bifurcation diagrams are analyzed to understand the qualitative changes in the system as the parameter α_2 is varied. Interestingly, the system exhibits significant dynamical changes in its behavior even with a very slight change in the parameter value, such as $\alpha_2 + 0.0001$. To investigate these dynamics, time-varying plots are simulated for each state variable of the proposed model (11). The parameter values used
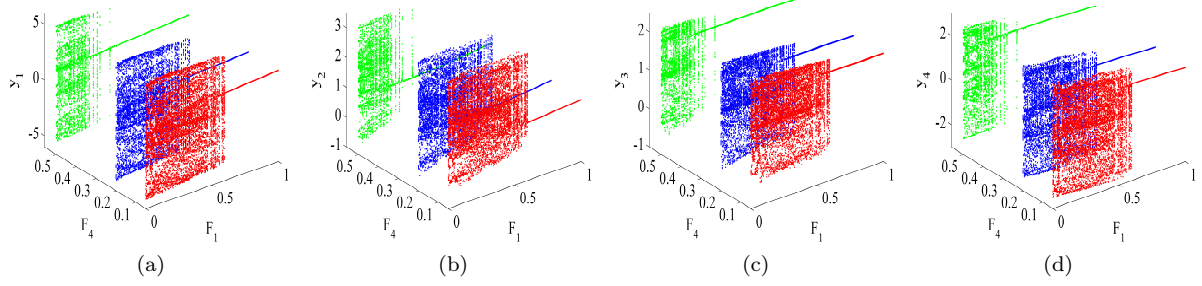
Fig. 23: Sequence of bifurcation diagrams for non-identical external stimulus $F_1 \neq F_4$.

for the simulation are as follows: $\alpha_1 = -0.5$, $\alpha_3 = 0.65$, $s_{12} = -0.4$, $s_{13} = 0.2$, $s_{14} = 3$, $s_{21} = -0.5$, $s_{23} = 1.3$, $s_{31} = 1$, $s_{32} = -0.9$, $s_{33} = 0.2$, $s_{41} = 1.4$ with initial state $(0.8, 0.3, 0.4, 0.6)$ and fractional order $\upsilon = 0.5$. The value of α_2 is varied starting from 0.3478 with an increment of $\alpha_2 + 0.0001$ till 0.3483 and the numerical outputs are displayed in Fig 24.

The sensitivity of the system to the parameter α_2 is evident from the changing patterns of oscillations observed in each state variable. The time-varying plots highlight a common behavior characterized by oscillations around two equilibrium states. As the value of α_2 increases, the time required for the transition between these states decreases. Additionally, the transient time between subsequent bursts of neurons varies for different values of α_2. In Figure 24(a), (b), (c), (d), it can be observed that the initial time taken for the firing pattern to appear is significantly longer compared to Figure 24(e) and (f).

7 Firing patterns and equilibrium shifting behavior

This section of the article aims to investigate the firing patterns exhibited by the neural network model and the switching behavior of the equilibria. The analysis is conducted in three different cases, each with distinct parameter choices, in order to gain a comprehensive understanding of the system's dynamics. One crucial aspect under discussion is the nature of equilibrium switching observed in the state variables. The study further compares the influence of external stimuli in the following sub-cases within each of the three main cases:

1. No external stimulus ($F_1 = F_4 = 0$).
2. Identical stimulus $F_1 = F_4 = 0.1$.
3. Non-identical stimulus $F_1 \neq F_4$
   – $F_1 = 0.1 < F_4 = 0.2$,
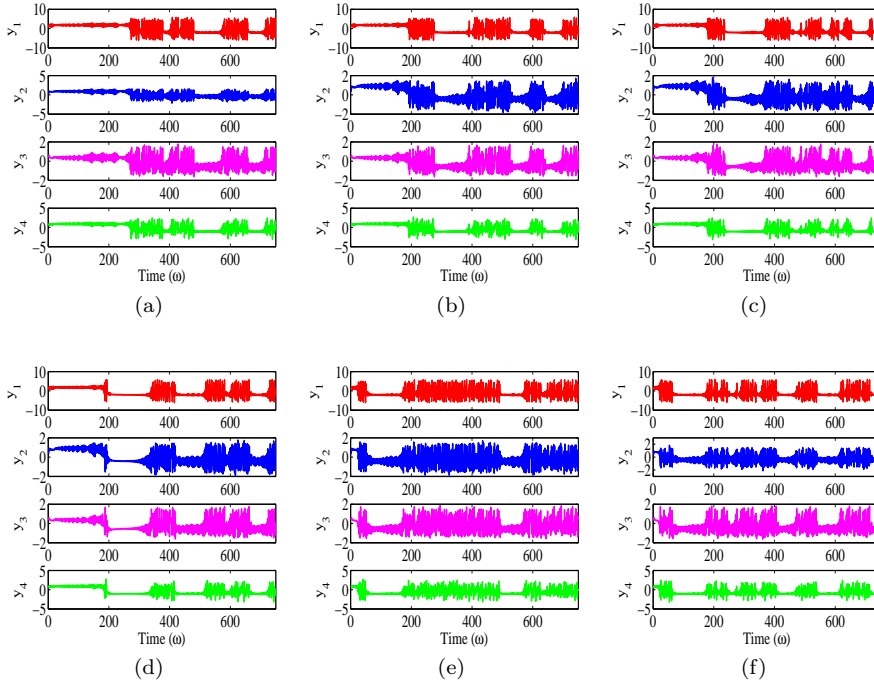   – $F_1 = 0.2 > F_4 = 0.1$.

Fig. 24: Phase plane plots illustrating sensitivity for (a) $\alpha_2 = -0.3478$ (b) $\alpha_2 = -0.3479$ (c) $\alpha_2 = -0.3480$ (d) $\alpha_2 = -0.3481$ (e) $\alpha_2 = -0.3482$ (f) $\alpha_2 = -0.3483$.

In order to bring in the factor of fractional order into the analysis, the study is performed for two different fractional orders $v = 0.5, 0.6$.

7.1 Case- I

In this specific scenario, the parameters are set as follows: $\alpha_1 = -0.5$, $\alpha_2 = 0.5$, $\alpha_3 = 0.65$, $s_{12} = -0.4$, $s_{13} = 0.2$, $s_{14} = 3$, $s_{21} = -0.5$, $s_{23} = 1.3$, $s_{31} = 0.5$, $s_{32} = -0.5$, $s_{33} = -0.2$, $s_{41} = 1.4$. The initial state is $(0.8, 0.3, 0.4, 0.6)$. In Figure 25, the oscillation patterns of each state variable are depicted, where (a), (b), (c), and (d) correspond to $v = 0.5$, and (e), (f), (g), and (h) correspond to $v = 0.6$. When $v = 0.5$, the system exhibits regular bursting behavior, with a shift in oscillation from the positive axis to the negative axis after a certain period of time. It is observed that the switch in oscillation takes a longer time when the external stimulus on neuron y_4 is higher than the stimulus on neuron y_1.
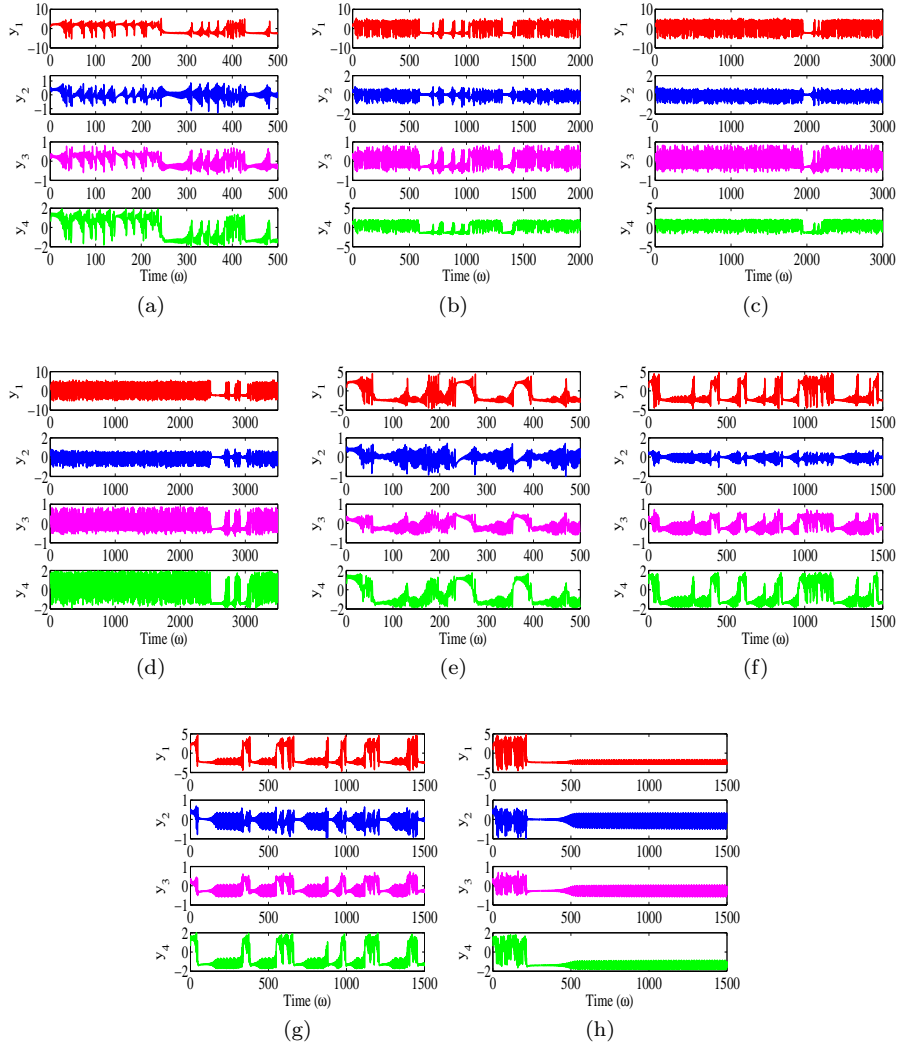
Fig. 25: Phase plane plots illustrating sensitivity for (a)$F_1 = F_4 = 0$, $v = 0.5$ (b) $F_1 = F_4 = 0.1$, $v = 0.5$ (c) $F_1 = 0.1 < F_4 = 0.2$, $v = 0.5$ (d) $F_1 = 0.2 > F_4 = 0.1$, $v = 0.5$ (e)$F_1 = F_4 = 0$, $v = 0.6$ (f) $F_1 = F_4 = 0.1$, $v = 0.6$ (g) $F_1 = 0.1 < F_4 = 0.2$, $v = 0.6$ (h) $F_1 = 0.2 > F_4 = 0.1$, $v = 0.6$.

7.2 Case- II

In this particular scenario, three parameters are varied while keeping the rest of the parameters fixed at the same values as in the previous case (Case - I). The modified parameter values are as follows: $\alpha_2 = 0.35$, $s_{31} = -0.5$, and

$s_{32} = -0.7$. The dynamics of the network model undergo significant changes compared to the previous case, as depicted in Figure 26.
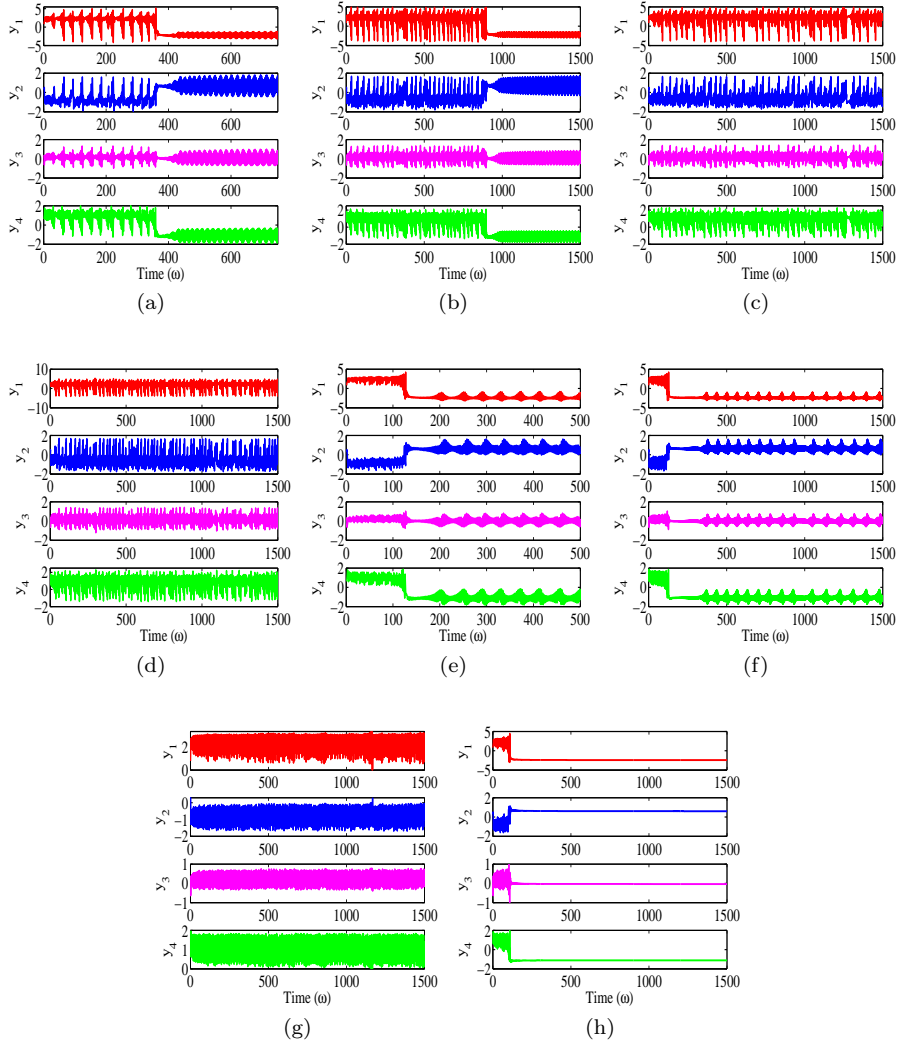
Fig. 26: Phase plane plots illustrating sensitivity for (a)$F_1 = F_4 = 0$, $\upsilon = 0.5$ (b) $F_1 = F_4 = 0.1$, $\upsilon = 0.5$ (c) $F_1 = 0.1 < F_4 = 0.2$, $\upsilon = 0.5$ (d) $F_1 = 0.2 > F_4 = 0.1$, $\upsilon = 0.5$ (e)$F_1 = F_4 = 0$, $\upsilon = 0.6$ (f) $F_1 = F_4 = 0.1$, $\upsilon = 0.6$ (g) $F_1 = 0.1 < F_4 = 0.2$, $\upsilon = 0.6$ (h) $F_1 = 0.2 > F_4 = 0.1$, $\upsilon = 0.6$.

It is evident from the figures that the system exhibits different patterns of behavior, including shifts in the oscillation axes. When there is no external
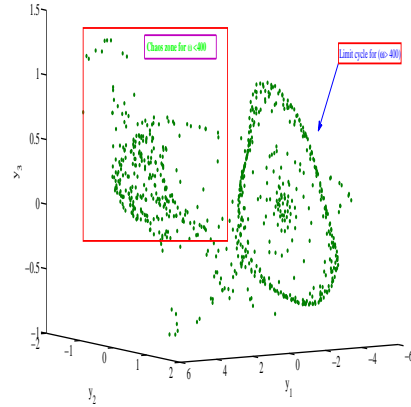
Fig. 27: Phase plane plot visualizing the shift in equilibrium for Case II corresponding to Fig 26(a).

stimulus or when identical stimuli close to zero are applied, the system displays a typical behavior, with the only difference being the time taken for the shift in the oscillation axis. The contrasting dynamics between $v = 0.5$ and $v = 0.6$ are evident in Figure 26(a), (b), (e), (f).

When the stimuli are non-identical, the system undergoes significant changes in behavior. For instance, when $F_1 < F_4$, the system exhibits a uniform bursting pattern along the positive axis (y_1, y_3, y_4) and the negative axis (y_2) as shown in Figure 26(c). However, when the stimuli are non-identical and $v = 0.6$, the system approaches stability, as seen in Figure 26(h), while the state variables undergo high regular bursting for $v = 0.5$ as depicted in Figure 26(d). To illustrate the equilibrium shift in the state variables, a 3D phase portrait corresponding to Figure 26(a) is presented in Figure 27. The uniform oscillations of the state variables after $\omega > 400$ lead to the formation of a closed-form spiral. The initial regular bursts are highlighted within the rectangular region in Figure 27.

7.3 Case- III

In this scenario, the parameter values remain the same as in Case - I, except for modifications in $s_{31} = -0.35$, $s_{32} = -0.7$, and $s_{33} = -0.4$. The visual analysis of the system's dynamics is presented in Figure 28.

Comparing this scenario with Case - I and Case - II, it is observed that the system undergoes a different dynamical change. The oscillations of the state variables switch between two equilibrium states, with a small region of stability in between, as depicted in Figure 28. Notably, when $F_1 > F_2$, the system achieves stability for both fractional orders $v = 0.5$ and $v = 0.6$. For

$\upsilon = 0.6$, the system exhibits similar behavior in all cases, starting with an initial burst followed by a stable region and a periodic oscillatory zone, except for the case when $F_1 > F_2$.

The qualitative change in behavior is further supported by the phase plane portrait corresponding to Figure 28(e), shown in Figure 29.
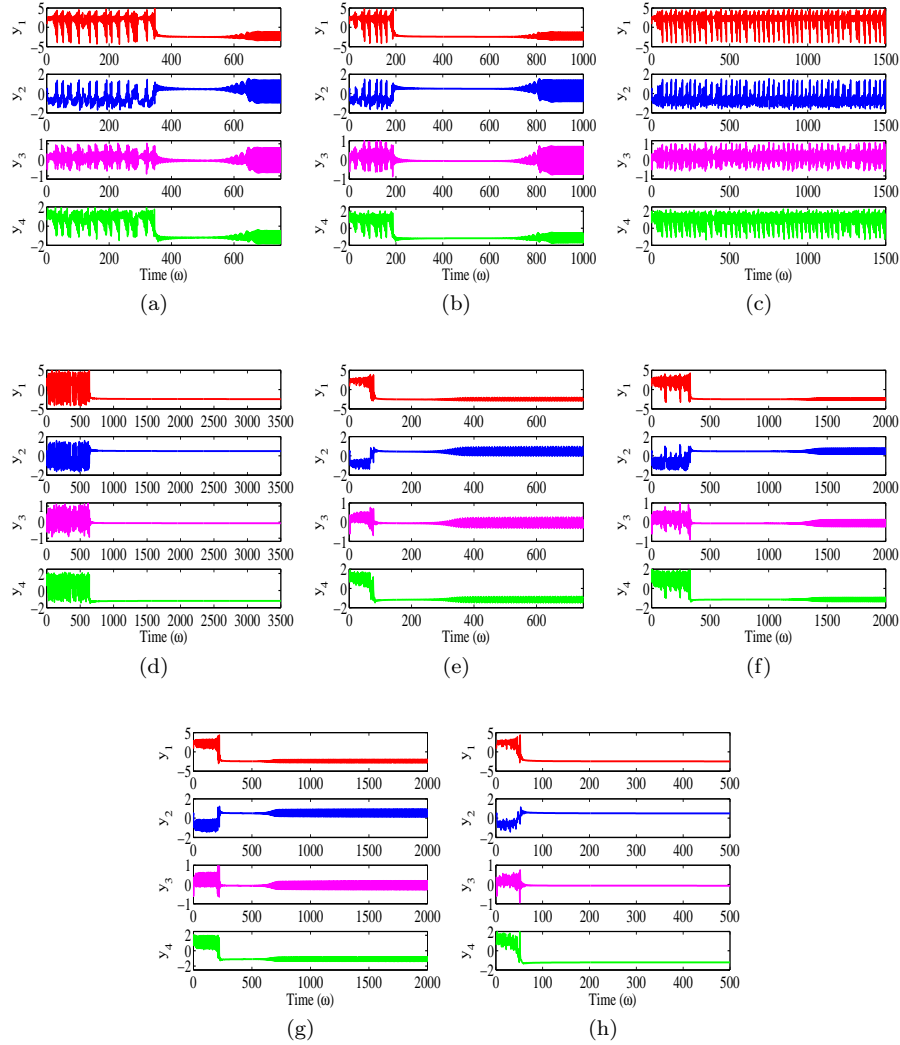

Fig. 28: Phase plane plots illustrating sensitivity for (a)$F_1 = F_4 = 0$, $\upsilon = 0.5$ (b) $F_1 = F_4 = 0.1$, $\upsilon = 0.5$ (c) $F_1 = 0.1 < F_4 = 0.2$, $\upsilon = 0.5$ (d) $F_1 = 0.2 > F_4 = 0.1$, $\upsilon = 0.5$ (e)$F_1 = F_4 = 0$, $\upsilon = 0.6$ (f) $F_1 = F_4 = 0.1$, $\upsilon = 0.6$ (g) $F_1 = 0.1 < F_4 = 0.2$, $\upsilon = 0.6$ (h) $F_1 = 0.2 > F_4 = 0.1$, $\upsilon = 0.6$.
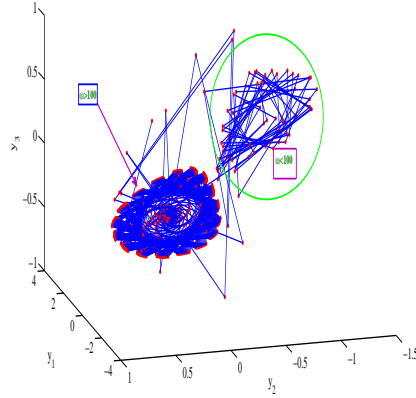
Fig. 29: Phase plane plot visualizing the shift in equilibrium for Case III corresponding to Fig 28(e).

Overall analysis of this section is tabulated in Table 3.

8 Conclusion

The findings of the study highlight an important observation regarding the impact of external stimuli on the system's behavior. It is observed that the absence of external stimuli leads to greater chaotic behavior compared to the presence of external stimuli. This observation underscores the role of external stimuli as a control factor in maintaining the system's stability. The bifurcation diagrams presented in Figures 7 and 18 support this conclusion by illustrating the zone of chaos and the transition of system states under parameter changes. The analysis of the system's behavior using Lyapunov exponents further provides evidence of nonlinear phenomena and bifurcations. Under the examined parameter values, the neural network model exhibits chaotic behavior for lower fractional orders. To achieve a broader representation of the neural model in various real-world settings, it is necessary to consider neurons with different activation functions.

Another intriguing characteristic investigated in this research is the capacity of the state variables to change equilibrium. This phenomenon reflects the biochemical processes within neurons, which can adjust their equilibrium locations to rectify errors that may occur during information transmission. The equilibrium shift is not constant and varies depending on the situation. The change in states can be continuous, as demonstrated in Figure 25(e), (f), (g), when neurons undergo frequent bursting. This exploration of different firing patterns provides insights into how neurons can dynamically restore their functional behavior. Overall, this study offers valuable insights into the

Table 3: Equilibrium shifting behavior analysis

Sub-case	Equilibrium states	Shift in states	Remarks
Case - I			
$F_1 = 0.1$ $F_4 = 0.1$	$P_1 = (-2.498, -0.023, -0.240, -1.268)$ $P_2 = (2.572, 0.165, 0.156, 1.206)$ $P_3 = (-0.093, -0.006, -0.036, -0.063)$	From P_2 to P_1	All state variables switch from positive to negative axis.
$F_1 = 0.1$ $F_4 = 0.2$	$P_1 = (-2.453, -0.024, -0.254, -1.213)$ $P_2 = (2.619, 0.164, 0.139, 1.264)$ $P_3 = (-0.173, -0.012, -0.066, -0.088)$	From P_2 to P_1	All state variables switch from positive to negative axis.
$F_1 = 0.2$ $F_1 = 0.1$	$P_1 = (-2.452, -0.024, -0.255, -1.335)$ $P_2 = (2.620, 0.144, 0.147, 1.145)$	From P_2 to P_1	All state variables switch from positive to negative axis.
Case - II			
$F_1 = 0.1$ $F_4 = 0.1$	$P_1 = (-2.471, 0.568, -0.041, -1.060)$ $P_2 = (-0.092, 0.122, -0.032, -0.045)$ $P_3 = (2.645, -0.948, 0.233, 0.938)$	From P_3 to P_1	y_1, y_3, y_4 switch from positive to negative axis y_2 from negative to positive axis.
$F_1 = 0.1$ $F_4 = 0.2$	$P_1 = (-0.168, 0.221, -0.057, -0.056)$ $P_2 = (-2.420, 0.610, -0.042, -1.007)$ $P_3 = (2.693, -0.894, 0.236, 0.981)$	No shift in states	y_1, y_2, y_3, y_4 oscillate about equilibrium P_3
$F_1 = 0.2$ $F_4 = 0.1$	$P_1 = (-2.432, 0.593, -0.039, -1.109)$ $P_2 = (-0.108, 0.141, -0.036, -0.081)$ $P_3 = (2.676, -0.898, 0.230, 0.896)$	No shift for $\upsilon = 0.5$ From P_3 to P_1 for $\upsilon = 0.6$	Oscillation about P_3 for $\upsilon = 0.5$ & y_1, y_3, y_4 switch from +ve to -ve axis y_2 from negative to positive axis for $\upsilon = 0.6$.
Case - III			
$F_1 = 0.1$ $F_4 = 0.1$	$P_1 = (-2.527, 0.451, -0.067, -1.141)$ $P_2 = (-0.087, 0.106, -0.031, -0.046)$ $P_3 = (2.697, -0.865, 0.242, 0.988)$	From P_3 to P_1	y_1, y_3, y_4 switch from positive to negative axis y_2 from negative to positive axis.
$F_1 = 0.2$ $F_4 = 0.1$	$P_1 = (-0.163, 0.196, -0.056, -0.058)$ $P_2 = (-2.480, 0.485, -0.071, -1.085)$ $P_3 = (2.745, -0.817, 0.241, 1.035)$	No shift for $\upsilon = 0.5$ From P_3 to P_2 for $\upsilon = 0.6$	Oscillation about P_3 for $\upsilon = 0.5$ & y_1, y_3, y_4 switch from +ve to -ve axis y_2 from negative to positive axis for $\upsilon = 0.6$.
$F_1 = 0.2$ $F_4 = 0.1$	$P_1 = (-2.487, 0.472, -0.068, -1.196)$ $P_2 = (-0.099, 0.118, -0.034, -0.082)$ $P_3 = (2.728, -0.817, 0.237, 0.944)$	From P_3 to P_1	Initial oscillation about P_3, attains stability about P_1.

qualitative properties of the investigated 4D model, emphasizing the role of external stimuli, the occurrence of bifurcations, and the ability of neurons to adapt and recover their equilibrium states in response to varying conditions.

Funding

Competing Interests

The authors have no relevant financial or non-financial interests to disclose.

Author Contributions

All authors contributed equally to the study conception and design. All authors read and approved the final manuscript.

Conflict of interest

The authors declare that they have no conflict of interest.

Data Availability

No datasets are generated or analysed during the current study.

References

1. Abbes, A., Ouannas, A., Shawagfeh, N., Khennaoui, A.A.: Incommensurate fractional discrete neural network: chaos and complexity. The European Physical Journal Plus **137**(2), 235 (2022)
2. Abdeljawad, T.: On Riemann and Caputo fractional differences. Computers & Mathematics with Applications **62**(3), 1602–1611 (2011)
3. Abdeljawad, T., Banerjee, S., Wu, G.C.: Discrete tempered fractional calculus for new chaotic systems with short memory and image encryption. Optik **218**, 163698 (2020)
4. Adeli, H.: Neural networks in civil engineering: 1989–2000. Computer-Aided Civil and Infrastructure Engineering **16**(2), 126–142 (2001)
5. Aguilar, C.Z., Gómez-Aguilar, J., Alvarado-Martínez, V., Romero-Ugalde, H.: Fractional order neural networks for system identification. Chaos, Solitons & Fractals **130**, 109444 (2020)
6. Aihara, K.: Chaos engineering and its application to parallel distributed processing with chaotic neural networks. Proceedings of the IEEE **90**(5), 919–930 (2002)
7. Alzabut, J., Tyagi, S., Abbas, S.: Discrete fractional-order bam neural networks with leakage delay: existence and stability results. Asian Journal of Control **22**(1), 143–155 (2020)
8. Atici, F., Eloe, P.: Initial value problems in discrete fractional calculus. Proceedings of the American Mathematical Society **137**(3), 981–989 (2009)
9. Bi, P., Hu, Z.: Hopf bifurcation and stability for a neural network model with mixed delays. Applied Mathematics and Computation **218**(12), 6748–6761 (2012)
10. Bishop, C.M.: Neural networks and their applications. Review of scientific instruments **65**(6), 1803–1832 (1994)

11. Čermák, J., Győri, I., Nechvátal, L.: On explicit stability conditions for a linear fractional difference system. Fractional Calculus and Applied Analysis **18**(3), 651–672 (2015)
12. Chen, J., Zeng, Z., Jiang, P.: Global mittag-leffler stability and synchronization of memristor-based fractional-order neural networks. Neural Networks **51**, 1–8 (2014)
13. Cheng, Z., Xie, K., Wang, T., Cao, J.: Stability and hopf bifurcation of three-triangle neural networks with delays. Neurocomputing **322**, 206–215 (2018)
14. Ge, J., Xu, J.: Stability and hopf bifurcation on four-neuron neural networks with inertia and multiple delays. Neurocomputing **287**, 34–44 (2018)
15. Goodrich, C., Peterson, A.C.: Discrete fractional calculus, vol. 10. Springer (2015)
16. Hioual, A., Ouannas, A., Oussaeif, T.E., Grassi, G., Batiha, I.M., Momani, S.: On variable-order fractional discrete neural networks: Solvability and stability. Fractal and Fractional **6**(2), 119 (2022)
17. Huang, C., Wang, H., Cao, J.: Fractional order-induced bifurcations in a delayed neural network with three neurons. Chaos: An Interdisciplinary Journal of Nonlinear Science **33**(3), 033143 (2023)
18. Kaslik, E., Sivasundaram, S.: Nonlinear dynamics and chaos in fractional-order neural networks. Neural Networks **32**, 245–256 (2012)
19. Li, L., Wang, Z., Li, Y., Shen, H., Lu, J.: Hopf bifurcation analysis of a complex-valued neural network model with discrete and distributed delays. Applied Mathematics and Computation **330**, 152–169 (2018)
20. Lin, H., Wang, C., Deng, Q., Xu, C., Deng, Z., Zhou, C.: Review on chaotic dynamics of memristive neuron and neural network. Nonlinear Dynamics **106**(1), 959–973 (2021)
21. Ma, T., Mou, J., Li, B., Banerjee, S., Yan, H.: Study on the complex dynamical behavior of the fractional-order hopfield neural network system and its implementation. Fractal and Fractional **6**(11), 637 (2022)
22. Magin, R.: Fractional calculus in bioengineering, part 1. Critical Reviews in Biomedical Engineering **32**(1) (2004)
23. Odom, M.D., Sharda, R.: A neural network model for bankruptcy prediction. In: 1990 IJCNN International Joint Conference on neural networks, pp. 163–168. IEEE (1990)
24. Ostalczyk, P.: Discrete fractional calculus: applications in control and image processing, vol. 4. World scientific (2015)
25. Ouannas, A., Khennaoui, A.A., Momani, S., Grassi, G., Pham, V.T.: Chaos and control of a three-dimensional fractional order discrete-time system with no equilibrium and its synchronization. AIP Advances **10**(4), 045310 (2020)
26. Petras, I.: A note on the fractional-order cellular neural networks. In: The 2006 IEEE International Joint Conference on Neural Network Proceedings, pp. 1021–1024. IEEE (2006)
27. Selvam, A.G.M., Baleanu, D., Alzabut, J., Vignesh, D., Abbas, S.: On Hyers–Ulam Mittag-Leffler stability of discrete fractional Duffing equation with application on inverted pendulum. Advances in Difference Equations **2020**(1), 1–15 (2020)
28. Shida, L., Shaoying, S., Shishi, L., Fuming, L.: The bridge between weather and climateâĂŤâĂŤfractional derivatives. Weather Technology **35**(1), 15–19 (2007)
29. Sierociuk, D., Petráš, I.: Modeling of heat transfer process by using discrete fractional-order neural networks. In: 2011 16th International Conference on Methods & Models in Automation & Robotics, pp. 146–150. IEEE (2011)
30. Sierociuk, D., Sarwas, G., Dzieliński, A.: Discrete fractional order artificial neural network. acta mechanica et automatica **5**(2), 128–132 (2011)
31. Song, C., Cao, J.: Dynamics in fractional-order neural networks. Neurocomputing **142**, 494–498 (2014)
32. Udhayakumar, K., Rihan, F.A., Rakkiyappan, R., Cao, J.: Fractional-order discontinuous systems with indefinite lkfs: An application to fractional-order neural networks with time delays. Neural Networks **145**, 319–330 (2022)
33. Vignesh, D., Banerjee, S.: Dynamical analysis of a fractional discrete-time vocal system. Nonlinear Dynamics **111**, 4501âĂŞ4515 (2023)
34. Vignesh, D., Banerjee, S.: Reversible chemical reactions model with fractional difference operator: Dynamical analysis and synchronization. Chaos: An Interdisciplinary Journal of Nonlinear Science **33**(3), 033126 (2023)
35. Wu, G.C., Abdeljawad, T., Liu, J., Baleanu, D., Wu, K.T.: Mittag-leffler stability analysis of fractional discrete-time neural networks via fixed point technique (2019)

36. Wu, G.C., Baleanu, D.: Jacobian matrix algorithm for Lyapunov exponents of the discrete fractional maps. Communications in Nonlinear Science and Numerical Simulation **22**(1-3), 95–100 (2015)
37. Xu, C., Mu, D., Liu, Z., Pang, Y., Liao, M., Li, P., Yao, L., Qin, Q.: Comparative exploration on bifurcation behavior for integer-order and fractional-order delayed bam neural networks. Nonlinear Analysis: Modelling and Control **27**, 1–24 (2022)
38. Yan, X.P.: Hopf bifurcation and stability for a delayed tri-neuron network model. Journal of Computational and Applied Mathematics **196**(2), 579–595 (2006)
39. Yang, Q., Chen, D., Zhao, T., Chen, Y.: Fractional calculus in image processing: a review. Fractional Calculus and Applied Analysis **19**(5), 1222–1249 (2016)
40. Yang, X.S., Yuan, Q.: Chaos and transient chaos in simple hopfield neural networks. Neurocomputing **69**(1-3), 232–241 (2005)
41. Zhang, L., Song, Q., Zhao, Z.: Stability analysis of fractional-order complex-valued neural networks with both leakage and discrete delays. Applied Mathematics and Computation **298**, 296–309 (2017)